

Thermal cycling stability of the martensitic transformation in $\text{Ti}_{40.7}\text{Hf}_{9.5}\text{Ni}_{49.8-x}\text{Cu}_x$ ($x = 1, 5$ or 10 at. %) cast alloys

N.N. Resnina ¹✉, S.P. Belyaev ¹, A.I. Bazlov ², A.V. Sibirev ¹,
I.V. Ponikarova ¹, M.E. Trofimova ¹, A.M. Ivanov ¹, R.M. Bikbaev ¹

¹ St. Petersburg State University, St. Petersburg, Russia

² National University of Science and Technology "MISIS", Moscow, Russia

✉ resnat@mail.ru

ABSTRACT

The martensitic transformation and the defect density variation were studied during 500 thermal cycles of the $\text{Ti}_{40.7}\text{Hf}_{9.5}\text{Ni}_{49.8-x}\text{Cu}_x$ shape memory alloys with various copper concentration ($x = 1, 5$ or 10 at. %). It was found that regardless the Cu content, the transformation temperatures decreased on thermal cycling. An increase in the Cu concentration led to alloys hardening but it did not improve thermal cycling stability. The variation in the defect density on thermal cycling did not correlate with the yield limit for dislocation slip measured in samples before cycling. The variation in the defect density variation did not correlate with the variation in the transformation temperatures on thermal cycling. This showed that the variation in defect density was not the only reason for the variation in the transformation temperatures on thermal cycling of cast Ti-Hf-Ni-Cu alloys.

KEYWORDS

shape memory alloys • thermal cycling stability • martensitic transformation • alloy hardening

Funding. This work has been supported by the grant of the Russian Science Foundation, RSF 23-19-00280.

Acknowledgements. The research was carried out using the equipment of the resource centers of the St. Petersburg State University Scientific Park "X-ray Diffraction research methods".

Citation: Resnina NN, Belyaev SP, Bazlov AI, Sibirev AV, Ponikarova IV, Trofimova ME, Ivanov AM, Bikbaev RM. Thermal cycling stability of the martensitic transformation in $\text{Ti}_{40.7}\text{Hf}_{9.5}\text{Ni}_{49.8-x}\text{Cu}_x$ ($x = 1, 5$ or 10 at. %) cast alloys. *Materials Physics and Mechanics*. 2025;53(1): 57–67.

http://dx.doi.org/10.18149/MPM.5312025_5

Introduction

NiTi-based shape memory alloys are the smart materials which are widely used in various technological branches. One of the most frequent applications is the actuators of repeat action which are applicable for car, aircraft, space and other industries [1–3]. The repeat action actuators usually consist of the pre-deformed shape memory alloy element which is connected to the elastic counter-body. On heating through the temperature range of the reverse martensitic transformation, the shape memory effect occurs and the strain recovers in the shape memory element. This leads to the deformation of the counter-body and the recovery stress appears in the system. On cooling through the temperature range of the forward martensitic transformation, the counter-body deforms the shape memory element, its strain increases, while the recovery stress decreases. On next heating, the described procedure repeats so, the recoverable strain and stress variation take place on thermal cycling [2,3]. For the actuators, the thermal cycling stability is the key factor



because the device must demonstrate the stable stress and strain variation in the same temperature range during the life-time period [4].

The NiTi-based shape memory alloys are the best candidates for the actuators because they demonstrate the best combination of the functional and operating properties such as high recovery strain and stress, high strength and corrosion resistance [5]. However, their thermal cycling stability is weak so, the recovery stress and strain as well as the temperatures of the strain and stress variation significantly change on thermal cycling [6–19]. Moreover, the plastic strain accumulates during thermal cycling that changes the geometrical sizes of the shape memory element and affects the recovery strain and stress [7,9,11,14]. The reason for the plastic strain accumulation is a high local stress appears on a growth of the martensite plate on cooling that leads to the local dislocation slip and increases the dislocation density [12,13,16–18]. One believes, that this is the reason for a weak thermal cycling stability of the martensitic transformation, that reveals as a decrease in the transformation temperatures of the forward and reverse transformations [12,13,16,18]. Thus, the alloy hardening, such as preliminary deformation, the precipitate hardening and a decrease in grain size is usually used to improve the thermal cycling stability of the martensitic transformation on thermal cycling of NiTi-based alloys [19–21].

The solid solution hardening is also used to improve the thermal cycling stability. Usually, the NiTi-based alloys are doped by third element, such, as Hf, Zr, Fe, Cu elements, which dissolve in the NiTi solid solution that increases the yield limit for dislocation slip. Last time, the quaternary Ti-Hf-Ni-Cu shape memory alloys were developed [22–27]. In [24,25], it was shown that the thermal cycling stability of the martensitic transformations in the cast Ti-Hf-Ni-Cu alloy with a 5 at. % of Hf and Cu atoms was better than in binary NiTi. In [27], it was found, that thin ribbons of Ti-Hf-Ni-Cu alloys with 9.5 at. % of Hf and various Cu content ($\text{Ti}_{40.7}\text{Hf}_{9.5}\text{Ni}_{44.8}\text{Cu}_5$ and $\text{Ti}_{40.7}\text{Hf}_{9.5}\text{Ni}_{39.8}\text{Cu}_{10}$) demonstrated the perfect thermal cycling stability of the B2 \leftrightarrow B19' transformation. The temperatures of the martensitic transformation were constant during 50 thermal cycles that had never been found for binary NiTi alloy. One may assume that perfect stability is caused by the solid solution hardening induced by the presence of the Hf and Cu atoms, which act as substitutional defects. On the other hand, the perfect thermal cycling stability may be attributed to a small grain size because thin ribbons had an average grain size of 800 nm in [27]. The aim of the present paper was to study the variation in the martensitic transformation and defect density variation on thermal cycling of cast $\text{Ti}_{40.7}\text{Hf}_{9.5}\text{Ni}_{48.8}\text{Cu}_1$, $\text{Ti}_{40.7}\text{Hf}_{9.5}\text{Ni}_{44.8}\text{Cu}_5$ and $\text{Ti}_{40.7}\text{Hf}_{9.5}\text{Ni}_{39.8}\text{Cu}_{10}$ alloys. This allows one to clarify the influence of the Cu concentration in cast $\text{Ti}_{40.7}\text{Hf}_{9.5}\text{Ni}_{49.8-x}\text{Cu}_x$ alloys on the alloy hardening and thermal cycling stability.

Materials and Methods

The $\text{Ti}_{40.7}\text{Hf}_{9.5}\text{Ni}_{49.8-x}\text{Cu}_x$ alloys ($x = 1, 5$ or 10 at. %) were produced in a vacuum arc furnace under an argon atmosphere purified by a Ti getter. The chemical composition of the alloy is correspond to the composition of the casting charge. High-purity single metals (99.9 wt. %) were used as raw materials. Each ingot with a mass of 20 g and a diameter

of 20 mm were turned over and remelted five times to obtain a homogeneous composition. For convenience, the alloys were labeled as Cu-1, Cu-5, Cu-10.

The structure was studied by X-ray diffraction (XRD) analysis at room temperature (Rigaku MiniFlex, $\text{CuK}\alpha$ radiation, θ - 2θ mode). The martensitic transformations were studied by differential scanning calorimetry (Mettler Toledo 822e) on cooling and heating in a temperature range from 200 to -100 °C with a rate of 10 °C/min. The resistivity (in the regime of the direct current) was measured by 4-probes technique on cooling and heating in the same temperature range using the self-made stand including two nano-voltmeters and one source of direct current. The samples for DSC study with a size of $3 \times 3 \times 1$ mm³ and samples for resistivity measurement with a size of $20 \times 1 \times 0.3$ mm³ were cut by electro-discharge machine from ingots.

The samples were subjected to 500 thermal cycles and the resistivity vs temperature curves were measured in the 1st, 10th, 20th, 30th, 40th, 50th, 75th, 100th, 200th, 300th, 400th and 500th cycles. Between these cycles, samples were thermal cycled by holding in the furnace at 200 °C for 40 s and holding in liquid nitrogen for 40 s.

To study whether the Cu content leads to alloy hardening, the samples were subjected to tension at a temperature of $A_f + 50$ °C (in the austenite state) before thermal cycling. Dog-bone samples with a size of gauge area of $7 \times 1 \times 0.8$ mm³ were cut by discharge machine from ingots, installed to the inter-grips which were fixed in the standard grips of the testing machine (Lloyd 30k Plus, Shimadzu 50kN-AG) equipped with a thermal chamber. The sample was heated to chosen temperature, hold for 40 min for homogenization of the temperature in the samples and grips and deformed by tension up to fracture. The stress was measured by standard cell, the strain was detected by video extensometer as the variation in distance between two white stripes drawn on the black sample surface.

Results and Discussion

Figure 1 shows the XRD patterns obtained at room temperature. The diffraction peaks of the B19' martensite phase can be observed, hence all alloys underwent the B2 \rightarrow B19' transformation on cooling to room temperature. Among the reflexes of main phase, weak reflexes of the Ti₂Ni-type precipitates were found.

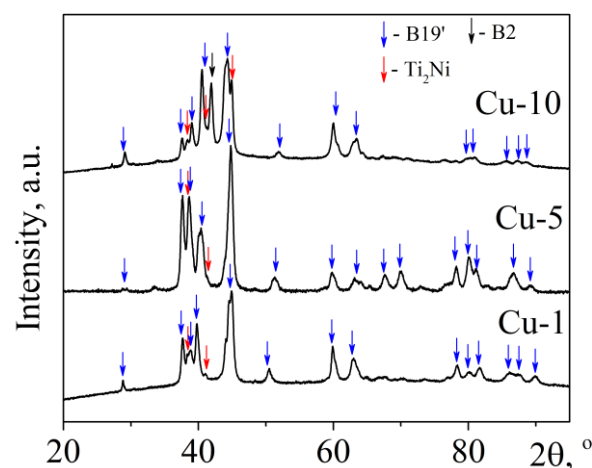


Fig. 1. XRD patterns of the Cu-1, Cu-5 and Cu-10 samples measured at room temperature

Figure 2 shows the calorimetric and resistivity curves found on the first cooling and heating of the $\text{Ti}_{40,7}\text{Hf}_{9,5}\text{Ni}_{49,8-x}\text{Cu}_x$ alloys. It is seen that in all samples, a peak of the heat release was found on cooling and a peak of heat absorption was observed on heating due to the $\text{B2} \leftrightarrow \text{B19}'$ transformation. In Cu-10 sample, the M_f temperature was less than room temperature that was why the austenite reflexes were observed on the XRD pattern (Fig. 1). The resistivity curves showed the anomalous behavior on cooling and heating: the resistivity increased on cooling due to the forward $\text{B2} \rightarrow \text{B19}'$ transformation; and it decreased on heating during the reverse $\text{B19}' \rightarrow \text{B2}$ transformation. It is seen that the temperatures of the anomalies on the $\rho(T)$ curves were the same as the temperatures of the peak on the calorimetric curves. Thus, using the $\rho(T)$ curves, one may determine the transformation temperatures as well as the absolute value of the resistivity which reflects the defect density.

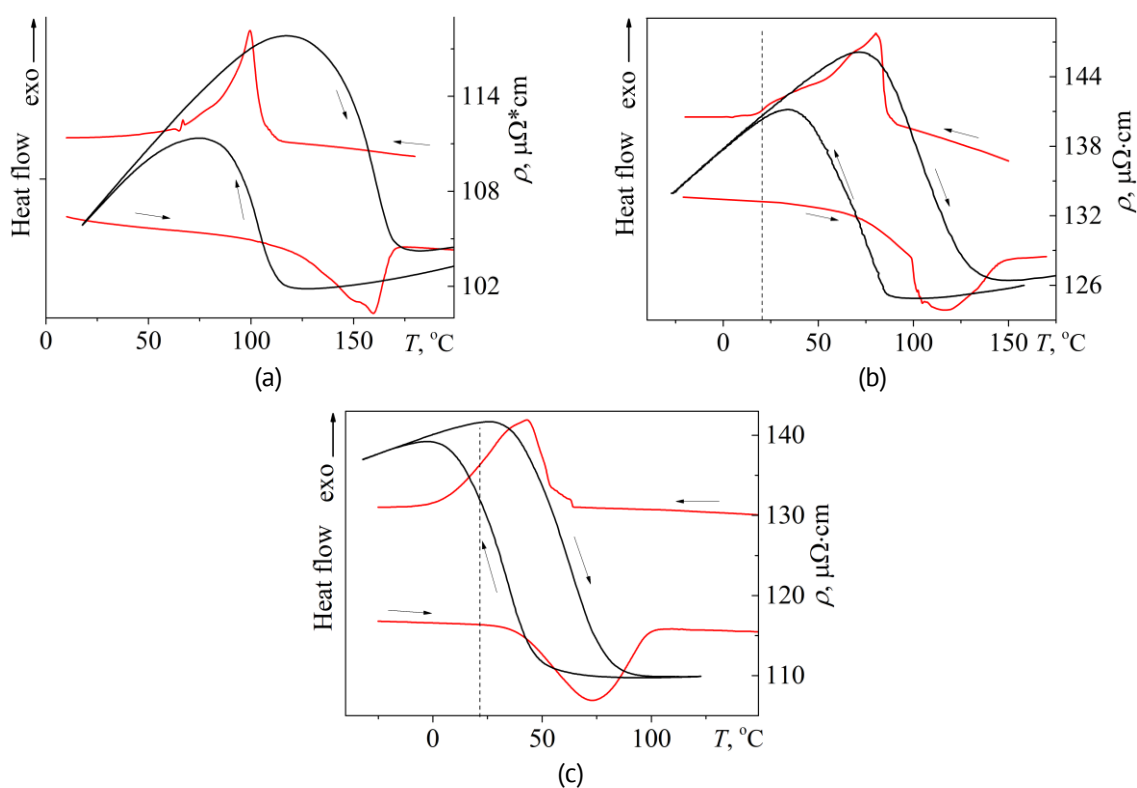


Fig. 2. The calorimetric (red) and resistivity (black) curves found on the first cooling and heating of the cast Cu-1 (a), Cu-5 (b) and Cu-10 (c) alloys. Dash line shows the room temperature

Figure 3 shows the $\rho(T)$ curves found in the 1st, 10th, 100th and 500th thermal cycles in the samples with various Cu content. It is seen that the $\rho(T)$ curves shifts on thermal cycling in different manner depending on Cu content. In Cu-1 alloy, an increase in thermal cycle number (N) from 1st to 100th shifted the $\rho(T)$ curves to high resistivity value and low temperatures. Further increase in cycle number to 500th cycle shifted the $\rho(T)$ curve to low resistivity (Fig. 3(a)). In Cu-5 and Cu-10 alloy, the $\rho(T)$ curves shifted to high resistivity value and low temperatures during 500 thermal cycles. However, it is seen that in Cu-5 alloy, the $\rho(T)$ curves measured in the 100th and 500th cycles were close to each other (Fig. 3(b)), hence the thermal cycling from the 100 to 500 cycles had a small effect

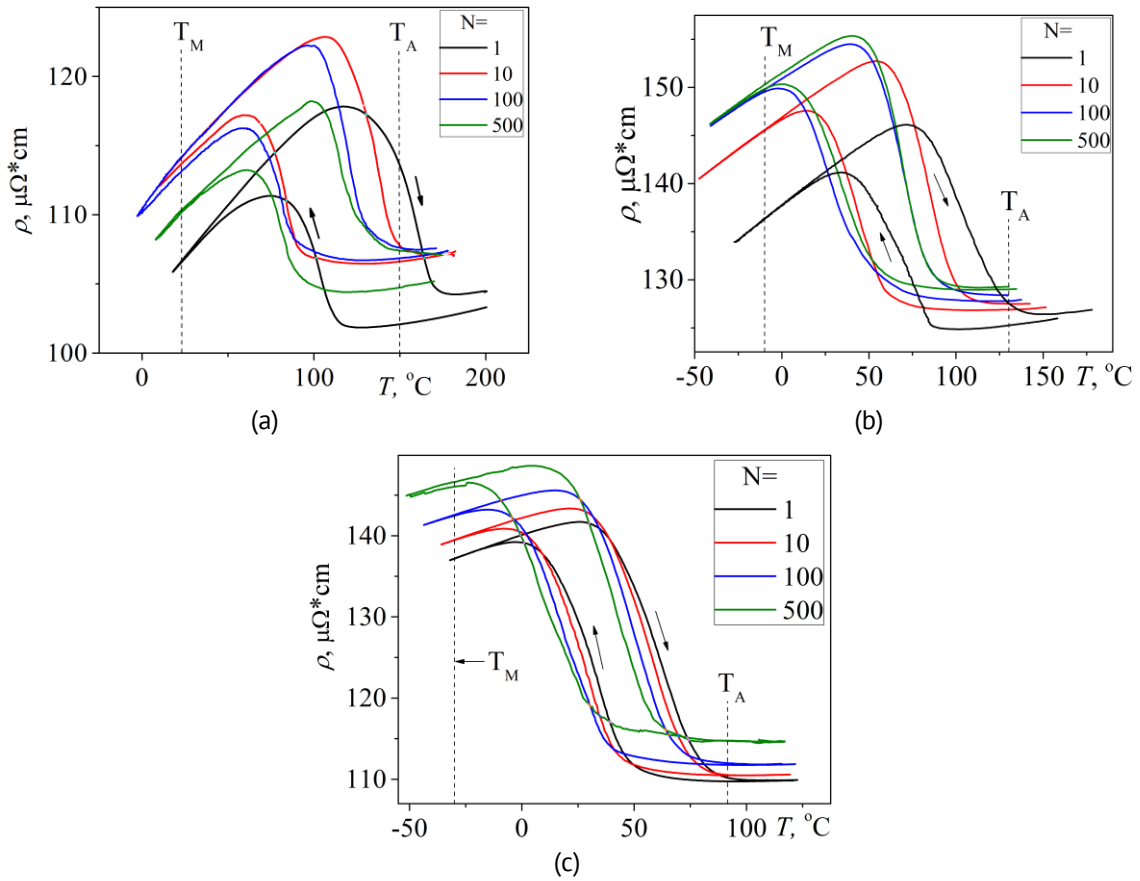


Fig. 3. The resistivity vs temperature curves measured for Cu-1 (a), Cu-5 (b) and Cu-10 (c) alloys in the 1st, 10th, 100th and 500th thermal cycle

on the defect density in this alloy. In Cu-10 alloy, thermal cycling from 100 to 500 cycles considerably shifted the $\rho(T)$ curve to high resistivity and low temperatures (Fig. 3(c)).

Using the $\rho(T)$ curves, the transformation temperatures were determined as intersection of tangent lines and their dependences on the thermal cycle number are given in Fig. 4. First of all, contrary to the results found for ribbons in [27], the cast alloys with the same chemical composition did not demonstrate the stability of the martensitic transformation temperatures on thermal cycling. In Cu-1 and Cu-5 alloys (Fig. 4(a,b)), the transformation temperatures decreased during the first 100–200 cycles and then slightly increased (the exception was found in Cu-5 alloy, where the A_f temperature and the M_f temperature were constant at $N > 200$). For instance, in Cu-1 alloy, the M_s temperature was equal to 113 °C in the 1st cycle to 90 °C in the 100th cycle and 92 °C in the 500th cycle. At the same time, the A_s temperature was equal to 136 °C in the 1st cycle, 102 °C in the 200th cycle and 106 °C in the 500th cycle. In Cu-5 alloy, the M_s temperature was equal to 79 °C in the 1st cycle, 52 °C in the 100th cycle and 55 °C in the 500th cycle. The A_s temperature was equal to 71 °C in the 1st cycle, 48 °C in the 200th and 51 °C in the 500th cycles. In Cu-10 alloy, the transformation temperatures decreased during 500 cycles without saturation (Fig. 4(c)). So, during 500 cycles, the M_s temperature dropped from 48 to 35 °C, whereas the A_s temperature decreased from 37 to 20 °C. Thus, it is seen that the different temperatures changes on thermal cycling in different ways and it is hardly affected by the Cu concentration. So, Cu-10 alloy showed the minimum variation

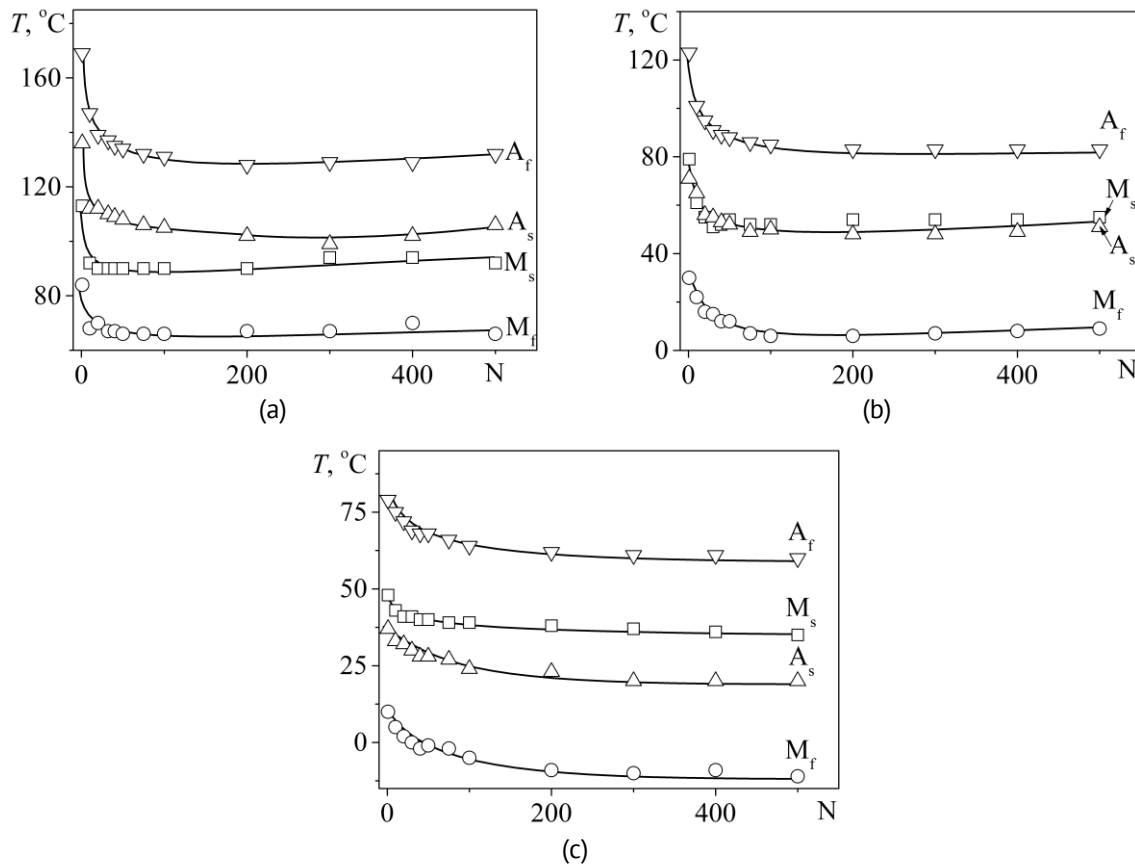


Fig. 4. The variation in transformation temperatures on thermal cycling of the Cu-1 (a), Cu-5 (b) and Cu-10 (c) alloys

in M_s temperature compared to the Cu-1 and Cu-5 samples, while the variation in the A_s temperature in Cu-10 and Cu-5 alloys were comparable and less than in Cu-1 alloy.

The resistivity values (ρ_A and ρ_M) were measured in a pure austenite state at the T_A temperature and pure martensite state at the T_M temperatures as shown by dash line in Fig. 3. As the absolute resistivity value depends on the defect density, hence the variation in the ρ_A and ρ_M values on thermal cycling shows the variation in defect density. The $\rho_A(N)$ and $\rho_M(N)$ curves for all samples are shown in Fig. 5. In Cu-1 sample, both the ρ_A and ρ_M values rapidly increase during first 10 cycles. The resistivity hardly changes from the 10th to the 100th cycle in the martensite state or from 10th to 200th cycle in the austenite state. At $N > 100$ (200) cycles, the resistivity decreases (Fig. 5(a)). The larger the Cu content in the alloy, the more cycles is taken for rapid increase in the resistivity. It occurs within 30 cycles in Cu-5 sample (Fig. 5(b)), and 80 cycles in Cu-10 sample (Fig. 5(c)).

To study the influence of the Cu content on the limit for dislocation slip, the samples were subjected to tension in the austenite state (at $T = A_f + 50$ °C) up to failure (Fig. 6) and the yield limit for dislocation slip was measured as $\sigma_{0.2}$ value. This value was equal to 480 MPa for Cu-1 alloy, 580 MPa for Cu-5 alloy and 730 MPa for Cu-10 alloy. According to SEM study which was not included in this paper, the volume fraction of precipitates did not change on a rise in the Cu concentration, hence an increase in $\sigma_{0.2}$ value on a rise in Cu content was caused by solid solution hardening.

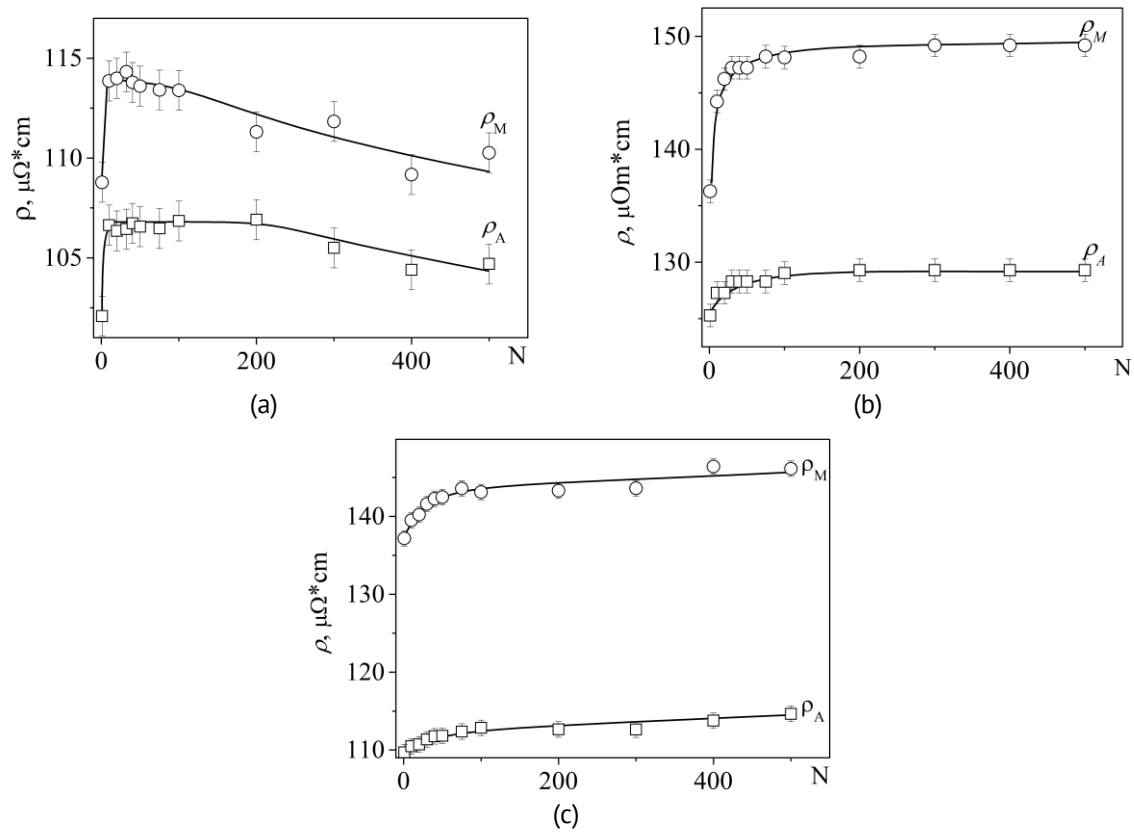


Fig. 5. The variation in the ρ_A and ρ_M values on thermal cycling of the Cu-1 (a), Cu-5 (b) and Cu-10 (c) alloys

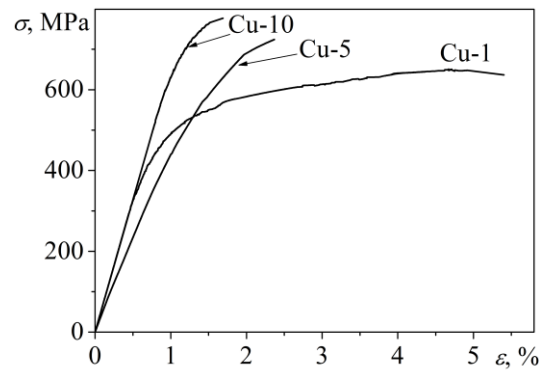


Fig. 6. Engineering stress vs strain curves of the Cu-1, Cu-5 and Cu-10 samples measured in the austenite state at $T = A_f + 50$ °C

The results of this study showed that the cast $\text{Ti}_{40.7}\text{Hf}_{9.5}\text{Ni}_{49.8-x}\text{Cu}_x$ alloys ($x = 5$ or 10 at. %) did not demonstrate the stability of the martensitic transformation contrary to the ribbons with the same composition which showed the perfect stability in [27]. One may assume that the main reason for different thermal cycling stability in cast and ribbon samples was the grain size which was $0.8 \mu\text{m}$ in ribbons and $130\text{--}150 \mu\text{m}$ in cast samples. The larger the grain size, the less the dislocation yield limit according to Hall-Petch law and the more intensive dislocation density variation on thermal cycling.

According to [18,28,29], an increase in dislocation density gives an additional term to the elastic energy which is included in the thermodynamic balance for the forward

martensitic transformation: $\Delta G^{A \rightarrow M} = E_d + E_{el}^{A \rightarrow M} + E_{el}^d$, where $\Delta G^{A \rightarrow M}$ is the increment in Gibbs energy during transformation, E_d is a dissipative energy which is responsible for hysteresis, $E_{el}^{A \rightarrow M}$ is an elastic energy stored during transformation, E_{el}^d is an elastic energy associated with the defect density [28]. If the defect density increases on thermal cycling, hence the E_{el}^d term increases and the larger increment in Gibbs energy must be provided to overcome the sum of dissipative and elastic energy and to start the martensitic transformation. This may be realized by overcooling that is why the start temperature of the martensitic transformation decreases on a rise in the defect density during thermal cycling.

One may assume that the dislocation density variation must depend on the yield limit for the dislocation slip ($\sigma_{0.2}$). It is obvious that in the alloys with a high $\sigma_{0.2}$ value, the variation in the defect density must be less than in the alloys with a low $\sigma_{0.2}$ value. Table 1 shows that an increase in the Cu concentration in the $\text{Ti}_{40.7}\text{Hf}_{9.5}\text{Ni}_{49.8-x}\text{Cu}_x$ alloys increases the yield limit for dislocation slip from 480 MPa in Cu-1 alloy to 730 MPa in Cu-10 alloy. So, one may expect that the variation in the defect density and the variation in the transformation temperatures must be the smallest in the Cu-10 sample and the largest in the Cu-1 alloy.

Table 1. Yield limit for dislocation slip, increment in the transformation temperatures, increment in ρ_M and ρ_A values during 500 cycles in $\text{Ti}_{40.7}\text{Hf}_{9.5}\text{Ni}_{49.8-x}\text{Cu}_x$ alloys

	Cu-1	Cu-5	Cu-10
$\sigma_{0.2}$, MPa	480	580	730
$\Delta\rho_M^{500}$, $\mu\Omega\cdot\text{cm}$	5.5	12.9	9
$\Delta\rho_A^{500}$, $\mu\Omega\cdot\text{cm}$	4.6	4	4.9
ΔM_s^{500} , $^{\circ}\text{C}$	-21	-24	-13
ΔM_f^{500} , $^{\circ}\text{C}$	-18	-21	-21
ΔA_s^{500} , $^{\circ}\text{C}$	-30	-20	-17
ΔA_f^{500} , $^{\circ}\text{C}$	-37	-40	-19

Table 1 shows that the variation in resistivity measured in the martensite state was larger than in the austenite state in all alloys. This may be due to the resistivity variation in the austenite state depends on the variation in density of dislocation and point defect, while the resistivity in the martensite is additionally affected by the martensite twin structure which also changes on thermal cycling [30].

The resistivity increment measured in the austenite state during 500 thermal cycles was comparable for all alloys. The minimum value was 4 $\mu\Omega\cdot\text{cm}$ in Cu-5 sample, while the maximum value of 4.9 $\mu\Omega\cdot\text{cm}$ was measured in Cu-10 alloy (Table 1). At the same time, the error in resistivity value was equal to 1.1 $\mu\Omega\cdot\text{cm}$ (measured as the error for indirect measurement taking into account the errors in the length, current and voltage measurements). This means that the variation in the defect density in the austenite state is the same for all alloys and it does not depend on the yield limit for dislocation slip.

In the martensite state, the maximum increment in the resistivity is found in Cu-5 sample which has the medium value of the yield limit for dislocation slip, while the minimum increment in the resistivity is observed in Cu-1 sample with the smallest yield limit for dislocation slip. Hence, there is no correlation between the alloy hardening and the variation in defect density measured in the martensite state. Thus, the results of the

study show that the variation in the defect density on thermal cycling does not depend on the yield limit for dislocation slip measured in the alloys before thermal cycling. One may assume that the $\sigma_{0.2}$ value also changes on thermal cycling that affects the variation in the defect density.

To find the relation between the defect density variation and the transformation temperature variation, the increments in the resistivity and temperatures were analysed. One may assume that if the most of the alloy is in the austenite state at the M_s and A_f temperatures, hence these temperatures must depend on the defect density in the austenite state. Contrary, the A_s and M_f temperatures at which most of the alloy is in the martensite state must be affected by the defect density in the martensite state. Table 1 shows that the variation in defect density in the austenite state is the same in all alloys however, the variations in the M_s and A_f temperatures in Cu-1 and Cu-5 alloys are approximately 1.8 times larger than in Cu-10 sample. In the martensite state, the minimum resistivity variation is found in Cu-1 alloy and the maximum value is observed in Cu5 alloy. At the same time, the M_f temperature is approximately the same in all alloys, while the variation in A_s temperature in Cu-5 and Cu-10 alloys is in 1.5 times less than in Cu-1 alloy. Thus, the results of the paper clearly show that the variation in the transformation temperatures on thermal cycling has no relation with the variation in the defect density.

The comparison of the transformation temperature increments and the yield limit for dislocation slip shows that there is no ratio between these parameters. So, as it was mentioned above, the increment of the M_f temperature was the same in Cu-1 and Cu-10 alloy, while the difference in yield limit for dislocation slip was 1.5 times. The A_f increment in Cu-1 and Cu-5 alloys was the same, whereas the yield limit for dislocation slip in Cu-5 alloy was 100 MPa higher than in Cu-1 alloy.

Thus, the results of the study show that the defect density variation and the transformation temperatures change independently on thermal cycling and their variation does not depend on the yield limit for dislocation slip measured in the sample before thermal cycling. First, this means that the defect density variation is not the only reason for the variation in the transformation temperatures on thermal cycling in the NiTi-based alloys. Other reasons must be found that affect the thermal cycling stability of the martensitic transformations in NiTi-based alloys. The other main result is that the yield limit for dislocation slip measured in the sample before thermal cycling does not reflect the stability of the transformation temperatures. Hence, the chosen of the NiTi-based alloy with a high dislocation yield limit for application does not guarantee the high thermal cycling stability of the functional properties.

Conclusions

Thermal cycling stability of the martensitic transformations was studied in cast $\text{Ti}_{40.7}\text{Hf}_{9.5}\text{Ni}_{49.8-x}\text{Cu}_x$ alloys with various Cu concentrations. The analysis of the variation in the transformation temperatures, defect density and the yield limit for dislocation slip was carried out. The obtained results may be summarized as follows:

1. The variation in transformation temperatures on thermal cycling are different for the $\text{Ti}_{40.7}\text{Hf}_{9.5}\text{Ni}_{49.8-x}\text{Cu}_x$ alloys with various Cu concentration. If Cu concentration in the














Ti_{40.7}Hf_{9.5}Ni_{49.8-x}Cu_x alloy is equal to 1 or 5 at. %, transformation temperatures decrease during 100–200 cycles and then slightly increase. If Cu concentration is equal to 10 at. %, transformation temperatures decreased during 500 cycles without saturation. At the same time, the absolute increment in the transformation temperature hardly depended on the Cu concentration.

2. An increase in the Cu concentration leads to alloy hardening that increases the yield limit for dislocation slip in the austenite phase more than 1.5 times. However, it hardly affects the thermal cycling stability in cast Ti_{40.7}Hf_{9.5}Ni_{49.8-x}Cu_x alloys

3. The variation in the defect density on thermal cycling does not correlate with the yield limit for dislocation slip measured in samples before cycling. The defect density variation measured in the austenite state is comparable in all alloys. The maximum defect density variation in the martensite state is found in the Cu-5 alloy with the medium yield limit for dislocation slip. The minimum defect density variation is observed in Cu-1 alloy with the smallest dislocation yield limit.

4. The change in the defect density does not correlate with the variation in the transformation temperatures on thermal cycling. This shows that the variation in defect density is not the only reason for the weak cycling stability of the martensitic transformation temperatures on thermal cycling of the NiTi-based alloys.

CRediT authorship contribution statement

Natalia N. Resnina  : conceptualization, writing – original draft; **Sergey P. Belyaev**  : conceptualization, writing – review & editing; **Andrey I. Bazlov**  : investigation; **Alexei V. Sibirev**  : investigation; **Irina V. Ponikarova**  : investigation; **Marina E. Trofimova**: investigation; **Aleksei M. Ivanov**  : investigation; **Rashid M. Bikbaev**  : investigation.

Conflict of interest

The authors declare that they have no conflict of interest.

References

1. Razov AI. Application of titanium nickelide-based alloys in engineering. *Phys. Met. Metal.* 2004;97(1): 97–126.
2. Jani JM, Leary M, Subic A, Gibson MA. A review of shape memory alloy research, applications and opportunities. *Mater. Design.* 2014;56: 1078–1113.
3. Priadko AI, Pulnev SA, Kovalev OO, Ilin IA. Rotary actuator control based on tensile force elements made of shape memory Cu–Al–Ni crystals when operated in a cyclic mode. *Materials Physics and Mechanics.* 2019;42(4): 407–414.
4. Tobushi H, Date K, Miyamoto K. Characteristics and development of Shape-memory alloy heat engine. *Journal of Solid Mechanics and Materials Engineering.* 2010;4(7): 1094–1102.
5. Otsuka K, Ren X. Physical metallurgy of Ti–Ni-based shape memory alloys. *Progress in Materials Science.* 2005;50(5): 511–678.
6. Miyazaki S, Igo Y, Otsuka K. Effect of thermal cycling on the transformation temperatures of Ti–Ni alloys. *Acta Metallurgica.* 1986;34(10): 2045–2051.
7. Furuya Y, Park YC. Thermal cyclic deformation and degradation of shape memory effect in Ti–Ni alloy. *Nondestructive Testing and Evaluation.* 1992;8–9(1–6): 541–554.
8. Matsumoto H. Transformation behaviour with thermal cycling in NiTi alloys. *Journal of Alloys and Compounds.* 2003;350(1–2): 213–217.

9. Eggeler G, Hornbogen E, Yawny A, Heckmann A, Wagner M. Structural and functional fatigue of NiTi shape memory alloys. *Materials Science and Engineering: A*. 2004;378(1–2): 24–33.
10. Resnina N, Belyaev S. Multi-stage martensitic transformations induced by repeated thermal cycling of equiatomic TiNi alloy. *Journal of Alloys and Compounds*. 2009;486(1–2): 304–308.
11. Jones NG, Dye D. Martensite evolution in a NiTi shape memory alloy when thermal cycling under an applied load. *Intermetallics*. 2011;19(10): 1348–1358.
12. Pelton AR, Huang GH, Moine P, Sinclair R. Effects of thermal cycling on microstructure and properties in Nitinol. *Materials Science and Engineering: A*. 2012;532: 130–138.
13. Zhang J, Somsen C, Simon T, Ding X, Hou S, Ren S, Ren X, Eggeler G, Otsuka K, Sun J. Leaf-like dislocation substructures and the decrease of martensitic start temperatures: A new explanation for functional fatigue during thermally induced martensitic transformations in coarse-grained Ni-rich Ti–Ni shape memory alloys, *Acta Materialia*. 2012;60(5): 1999–2006.
14. Belyaev S, Resnina N, Sibirev A. Peculiarities of residual strain accumulation during thermal cycling of TiNi alloy. *Journal of Alloys and Compounds*. 2012;542: 37–42.
15. Kus K, Breczko T. Change in the transformation sequence due to stress-free thermal cycling of Ni-Ti shape memory alloy. *Materials Physics and Mechanics*. 2012;13: 64–69.
16. Churakova A, Gunderov D. Increase in the dislocation density and yield stress of the Ti₅₀Ni₅₀ alloy caused by thermal cycling. *Mater. Today: Proc.* 2017;4(3): 4732–4736.
17. Sibirev A, Resnina N, Belyaev S. Relationship between the variation in transformation temperatures, resistivity and dislocation density during thermal cycling of Ni₅₀Ti₅₀ shape memory alloy. *International Journal of Materials Research*. 2019;110(5): 387–392.
18. McCormick P, Liu Y. Thermodynamic analysis of the martensitic transformation in NiTi-II. Effect of transformation cycling. *Acta Metallurgica et Materialia*. 1994;42(7): 2407–2413.
19. Tong YX, Guo B, Chen F, Tian B, Li L, Zheng YF, Prokofiev EA, Gunderov DV, Valiev RZ. Thermal cycling stability of ultrafine-grained TiNi shape memory alloys processed by equal channel angular pressing. *Scripta Materialia*. 2012;67(1): 1–4.
20. Churakova A, Gunderov D. Microstructural and Mechanical Stability of a Ti-50.8 at. % Ni Shape Memory Alloy Achieved by Thermal Cycling with a Large Number of Cycles. *Metals*. 2020;10(2): 227.
21. Churakova A, Kayumova E, Gunderov D, Magomedova D. Interrelation of microstructure and kinetics of martensitic transformations in TiNi alloy in different structural states under thermal cycling conditions. *AIP Conf. Proc.* 2022;2533: 020049.
22. Resnina N, Belyaev S, Shelyakov A. Martensitic transformation in amorphous-crystalline Ti-Ni-Cu and Ti-Hf-Ni-Cu thin ribbons. *Eur. Phys. J. Spec. Top.* 2008;158: 21–26.
23. Denowh CM, Miller DA. Thermomechanical training and characterization of Ni–Ti–Hf and Ni–Ti–Hf–Cu high temperature shape memory alloys. *Smart Materials and Structures*. 2012;21(6): 065020.
24. Baradari S, Resnina N, Belyaev S, Nili-Ahmadabadi M. Martensitic phase transformation and shape memory properties of the as-cast NiCuTiHf and NiCuTiHfZr alloys. *Journal of Alloys and Compounds*. 2021;888: 161534.
25. Baradari S, Resnina N, Belyaev S, Nili-Ahmadabadi M. Cyclic Stability of Ni_{44.8}Cu₅Ti_{45.2}Hf₅ and Zr-Substituted Ni_{44.8}Cu₅Ti_{40.2}Hf₅Zr₅ Medium-Entropy Shape Memory Alloys. *Advanced Engineering Materials*. 2022;24(10): 2200106.
26. Li J, Yi X, Meng X, Qiao S, Cai W, Zhao L. Deposition and phase transformation behaviors of Ti-Ni-Hf-Cu quaternary shape memory alloy thin films. *Journal of Alloys and Compounds*. 2019;806: 33–39.
27. Resnina N, Belyaev S, Shelyakov A, Ubyivovk E, Ponikarova A. Stability of the B2 ↔ B19' martensitic transformation on thermal cycling of Ti-Hf-Ni-Cu thin ribbons. *Materials Letters*. 2024;357: 135770.
28. Salzbrenner RJ, Cohen M. On the Thermodynamics of Thermoelastic Martensitic Transformations. *Acta Metallurgica*. 1979;27: 739–748.
29. Wollants P, Roos JR, Delaey L. Thermally- and stress-induced thermoelastic martensitic transformations in the reference frame of equilibrium thermodynamics. *Progress in Materials Science*. 1993;37(3): 227–288.
30. Sibirev A, Ubyivovk E, Belyaev S, Resnina N. In situ transmission electron microscopy study of martensite boundaries movement on cooling and heating of the NiTi shape memory alloy. *Materials Letters*. 2022;319: 132267.